

## Evidence of two-stage melting of Wigner solids

Talbot Knighton, Zhe Wu, and Jian Huang\*


*Department of Physics and Astronomy, Wayne State University, Detroit, Michigan 48201, USA*

Alessandro Serafin and J. S. Xia

*National High Field Magnetic Laboratory, Tallahassee, Florida 32310, USA*

L. N. Pfeiffer and K. W. West

*Department of Electrical Engineering, Princeton University, Princeton, New Jersey 08544, USA*

 (Received 10 September 2017; revised manuscript received 11 November 2017; published 20 February 2018)

Ultralow carrier concentrations of two-dimensional holes down to  $p = 1 \times 10^9 \text{ cm}^{-2}$  are realized. Remarkable insulating states are found below a critical density of  $p_c = 4 \times 10^9 \text{ cm}^{-2}$  or  $r_s \approx 40$ . Sensitive dc  $V$ - $I$  measurement as a function of temperature and electric field reveals a two-stage phase transition supporting the melting of a Wigner solid as a two-stage first-order transition.

DOI: [10.1103/PhysRevB.97.085135](https://doi.org/10.1103/PhysRevB.97.085135)

A Wigner crystal (WC) [1] of electrons in two dimensions is a long-sought-after phenomenon driven by strong electron-electron interaction and the melting of a WC provides a unique opportunity of understanding the solid-liquid transition (SLT) [2–4]. According to the Monte Carlo calculations, a WC occurs when the ratio of the interparticle Coulomb energy  $E_{ee}$  and the Fermi energy  $E_F$ ,  $r_s = E_{ee}/E_F = a/a_B$ , is at least 37 [5].  $a = 1/\sqrt{\pi n}$  is the Wigner-Seitz radius for electron density  $n$  and  $a_B = \hbar^2\epsilon/m^*e^2$  is the Bohr radius. Therefore, in order to observe a WC, the charge concentrations must be extremely dilute, i.e.,  $\leq 1 \times 10^9 \text{ cm}^{-2}$  for electrons or  $\leq 4 \times 10^9 \text{ cm}^{-2}$  for holes in GaAs two-dimensional (2D) systems. Experiments in such small electron energy limits are challenging because the disorder effects, unless effectively suppressed, easily overwhelm the interaction-driven effects. Natural consequences are the Anderson localization [6], glass states [7], and mixed phases; all of which do not possess true long-range correlations. As a result, neither a WC nor a melting transition has been clearly demonstrated. Most detection efforts target collective modes and have so far produced only softly pinned modes undergoing a second-order-like thermal melting. These modes, as broadly suspected, could easily result from intermediate or mixed phases (e.g., hexatics, bubbles/stripes, or glass phases) since the observed correlation lengths ( $\xi$ ), corresponding to the sizes of WCs, are usually small. Clear evidence of a WC demands not only demonstrations of longer or even macroscopic  $\xi$ , but, moreover, a melting transition marked by a singularity [8–10]. This work presents evidence for collective pinning modes characterized by a macroscopic  $\xi$ , as well as two-stage SLT, analogous to the Kosterlitz-Thouless (KT) model [4,10–15], except for a first-order transition suggested by a discontinuity across the critical point.

Most WC studies adopt the reentrant and quantum Hall insulating phases (RIP and QHIP) in a large magnetic field

( $B$ ) where interaction effect is enhanced without reaching an ultradilute limit. Detection of the collective modes has been conducted with respect to pinning [16–18] and resonant absorption (via rf, microwaves, acoustic waves [19–22], tunneling [23]). However, there lacks evidence distinguishing a WC from intermediate/mixed phases. In fact, the estimated  $\xi$  is not only small (up to  $1 \mu\text{m}$ ), but also decays exponentially with increasing temperature ( $T$ ) in a fashion similar to what is expected for an intermediate phase (i.e., hexatics [13,24]). Similar results are also obtained through studies in zero- $B$  fields [25–27]. Zero- $B$  results at  $r_s > 40$  are quite rare due to the requirement for far more dilute carrier densities where disorder effect is even more prominent because the screening effect is weak as the interparticle spacing,  $a = 1/\sqrt{\pi n} \sim 200$ – $500 \text{ nm}$ , approaches the screening length. This is why even fairly clean systems become highly insulating when  $n$  is  $\sim 8$ – $9 \times 10^9 \text{ cm}^{-2}$  [27,28]. Consequently,  $r_s$  is limited to 5–15. Therefore, disorder suppression, as supported by almost all experiments, remains the key to successful detection of WCs.

In addition to driving a localization, another subtle disorder effect is its influence on the WC melting temperature ( $T_m$ ), i.e. via fluctuations that break long-range translational symmetry. This less understood effect could alter current models of melting such as the KT model and is expected to be more effective in suppressing  $T_m$  than the quantum fluctuations [9,10]. Disorder suppression is therefore key in keeping  $T_m$  accessible. Most reported  $T_m \sim 100$ – $200 \text{ mK}$  for small  $\xi$  cases are likely the crossover points between the intermediate/mixed and the liquid phases. To probe a transition, i.e., from a WC-intermediate phase, requires cooling to lower  $T$ .

This study focuses on the dc transport response of collective pinning and melting in ultrahigh-quality dilute 2D systems. A proven cooling method using a helium-3 immersion cell is adopted [29]. Key observations include enormously pinned collective modes, characterized by a differential resistance ( $r_d$ ) of  $\sim 1.3 \text{ G}\Omega$ , that exhibit a remarkable threshold nonlinear dc  $I$ - $V$  identical to pinned charge density waves (CDWs). The

\*Corresponding author: [jianhuang@wayne.edu](mailto:jianhuang@wayne.edu)

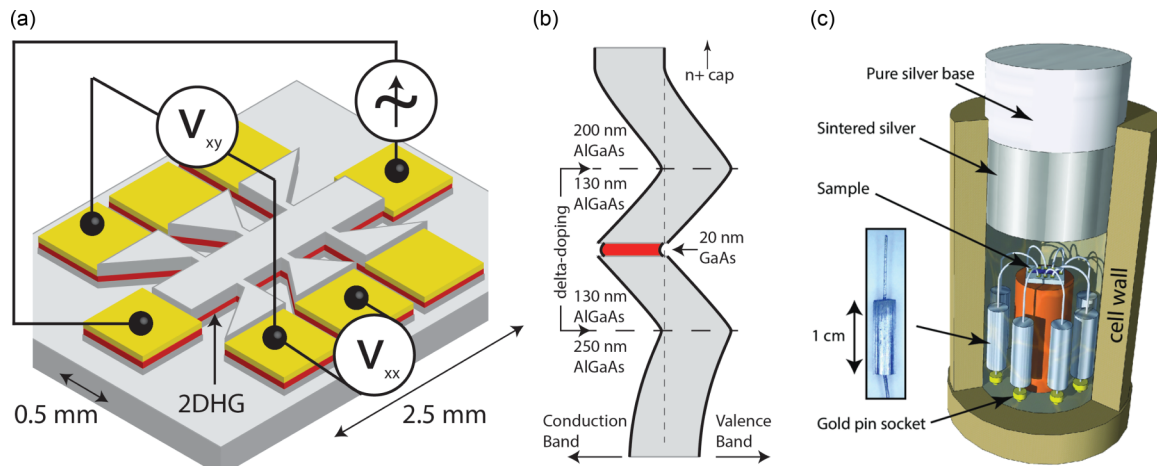


FIG. 1. (a) Sample dimensions and measurement configuration. (b) Band diagram of the quantum square well. (c) Cooling schematics inside a helium-3 immersion cell.

critical temperature is  $T_m \sim 35$  mK. Moreover, heating across  $T_m$  results in a discontinuity in  $r_d$  which supports a first-order two-stage thermal melting. The presentation is divided into two parts: The first is a study of the RIP near filling  $\nu = 1/3$  using  $p$ -doped quantum wells, and the second is a zero- $B$ -field study of ultradilute holes in undoped heterojunction-insulated-gate field-effect transistors (HIGFETs) at  $r_s \geq 40$ .

The samples used for the RIP measurement are lightly doped  $p$ -type (100) GaAs quantum wells patterned into a  $2.5 \times 0.5$  mm Hall bar. The density  $p$  is  $\sim 4 \times 10^{10}$  cm $^{-2}$  ( $r_s = 24$ ), with mobility of  $\mu \approx 2.5 \times 10^6$  cm $^2$ /V s. Thermally deposited AuBe pads annealed at 460 °C achieve excellent Ohmic contacts to the 2D carriers, with measured contact resistances  $\sim 400$   $\Omega$ . Measurements are performed in a dilution refrigerator inside a shielded room, allowing minimal electronic noises.

Cooling dilute carriers to 10 mK is challenging because sample thermalization relies mainly on cooling through the sample leads (via  $ee$  interaction) because the phonon modes are frozen out. We have established an effective cooling method via a helium-3 sample immersion cell and achieved 5 mK cooling GaAs 2D holes as dilute as  $p = 5 \times 10^9$  cm $^{-2}$  [29]. The carrier density for the RIP study here is nearly ten times higher. The cell is mounted at the lower end of a cold finger with its top fastened to the mixing chamber (mc) plate [Fig. 1(c)]. The roof is a sintered silver cylindrical-block extension made by compressed pure silver microparticles. During operation, helium-3 gas is continuously fed through a capillary into the cell where it condenses to fill the volume completely. Saturated sintered silver block provides  $\sim 30$  m $^2$  contact area to cool the helium-3 bath. Major cooling of the 2D holes is realized via efficiently heat-sinking the metal contacts through sintered silver pillars providing 2.5 m $^2$  surface area per lead.  $T$  is monitored through a helium-3 melting curve thermometer. The  $T$  differential between the bath and the mc is  $\leq 0.1$  mK at all times.

Figure 2(a) shows the magnetoresistance (MR) ( $\rho_{xx}$ ) and the Hall resistance ( $\rho_{xy}$ ) measured at 10 mK via a four-terminal ac technique. The inset shows the Shubnikov de Haas (SdH) oscillations starting at 0.05 T. The RIP peak centers at  $B = 4.5$  T ( $\nu = 0.375$ ) between fillings  $\nu = 2/5$  and  $1/3$ , with a dip

in  $\rho_{xy}$  consistent with previous studies [30,31].  $B = 4.5$  T corresponds to a magnetic length  $l_B = \sqrt{\hbar c/eB} \approx 28$  nm equal to  $a = 1/\sqrt{\pi p}$ . This is where a WC is expected. However, we found that dc techniques, instead of the ac techniques, are the appropriate method probing the RIP peak because, as shown later, it is essential to measured bulk resistance  $r$  with currents of  $\sim 1$  pA which are far below the offset limits in the ac driving signals. An electrometer-level dc setup is therefore adopted with a voltage bias  $V$  between  $\pm 10$  mV (at 0.1  $\mu$ V resolutions). Current sensing via a low-noise preamp provides 50 fA precision.

Cooling to 9 mK, dc  $IV$  within a  $\pm 5$  nA window displays a sharp threshold [inset of Fig. 2(b)] apparently identical to a pinned CDW [32]. The differential resistance  $r_d = dV/dI$  within the threshold  $V_c \sim 1$  meV is approximately 1.3 G $\Omega$ , with nearly no current flow ( $I \leq 1-2$  pA). This supports a collective pinning below a threshold electric field  $E_c = V_c/L \sim 10$  mV/cm because the single-particle energy  $w_c = eE_c a \sim 0.024$   $\mu$ eV (or 0.3 mK) is significantly smaller than  $T$ .  $L \sim 0.5$  mm is the distance between the voltage leads and  $a = 1/\sqrt{\pi p} = 28$  nm is the average charge spacing. However, current is switched on immensely at a critical current  $I_c$  and  $r_d$  plummets by nearly 6000 times. It indicates a phase transition occurring at a remarkably small threshold current  $I_c \sim 2$  pA. This electric field ( $E$ )-driven phase transition becomes more evident in the later  $T$ -dependent results. Joule heating is  $< 10^{-15}$  W and thus negligible.

Another important evidence that supports a crystal phase is a melting transition which several studies have reported around 150–300 mK [16–23,25–27]. Figure 2(b) shows  $IV$ s with each of the curves corresponding to a fixed  $T$  between 10 and 300 mK. The threshold behavior is robust up to  $\sim 40$  mK, with  $r_d \sim 1-1.3$  G $\Omega$  and  $I_c \sim 2-3$  pA. For higher  $T$ , the threshold behavior is replaced with rounded nonlinear  $IV$ s between 40 and 140 mK with substantially suppressed  $r_d \sim$  M $\Omega$ . Eventually, linear  $IV$  is restored beyond 140 mK which is commonly recognized as a liquid phase due to the absence of pinning.

Naturally, a phase transition can be driven by both  $T$  and  $I$  (or  $V$ ). Therefore, caution must be taken when examining the thermal melting because the sheet resistance  $r = V/I$  are

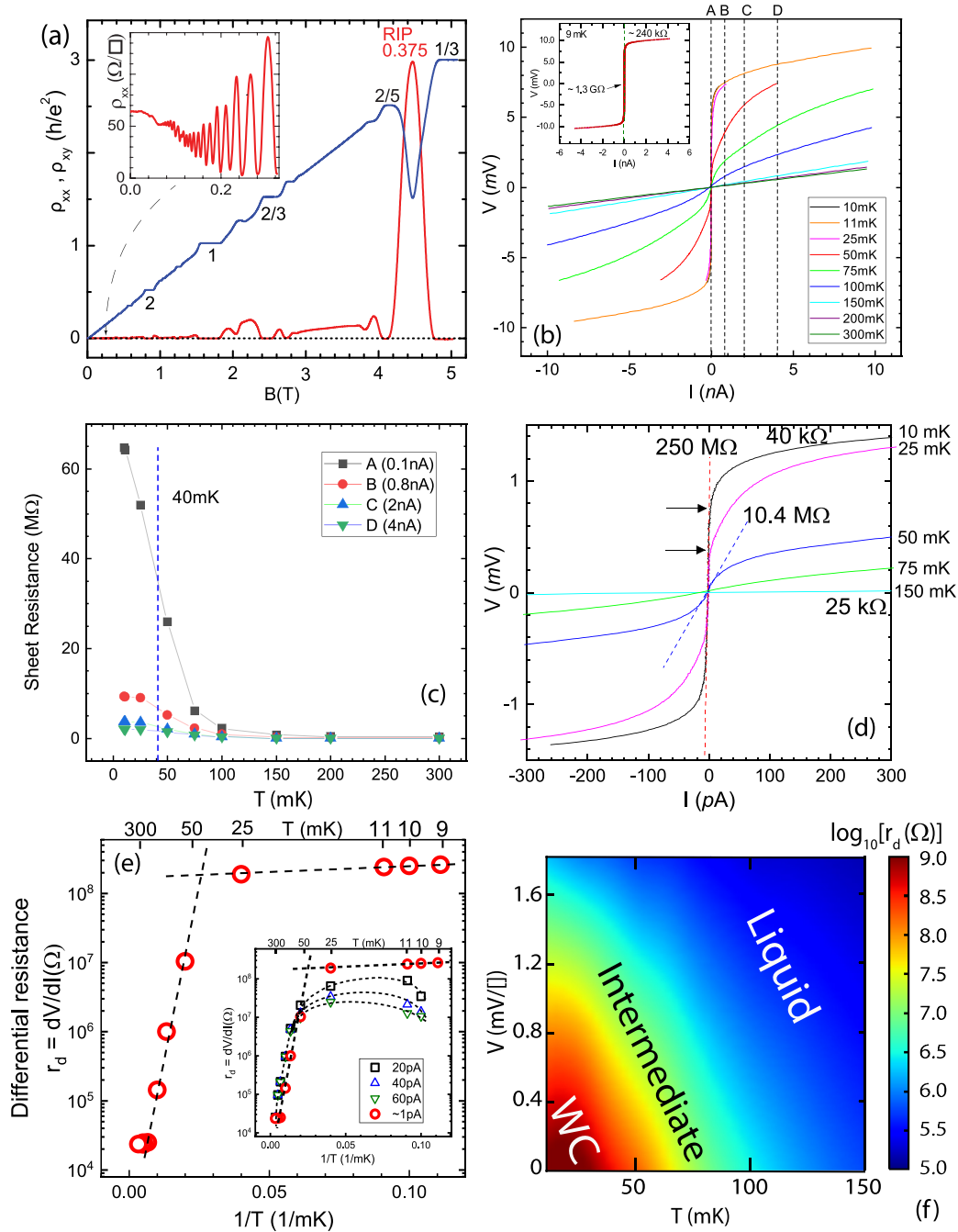


FIG. 2. (a) MR and Hall resistance at 10 mK. Inset: SdH oscillations. (b) dc  $IV$  measured at  $B = 4.5$  T at various  $T$  from 10 to 300 mK. Inset:  $IV$  at 9 mK. (c)  $T$  dependence of the resistance ( $V/I$ ) measured with 0.1, 0.8, 2, and 4 nA driving currents. (d) Amplified view of (b) for a narrower current range. (e) Piecewise  $T$  dependence of  $r_d(T) = dV/dI|_{V \rightarrow 0}$  on semilogarithmic scales. Inset: comparison to  $r_d(T)$  obtained with higher current drives. Dotted lines are guides. (f) Suggested contour phase diagram based on  $\log_{10} r_d(T)$  values.

extremely sensitive to the level of the drives down to picoampere limits. For a demonstration,  $r(T)$ s obtained at four different randomly picked current drives, labeled by the dotted lines in Fig. 2(b), are plotted in Fig. 2(c). For  $I \geq 1$  nA,  $r(T)$  varies little with increasing  $I$ , consistent with a liquid phase behavior. However,  $r(T)$  exhibits more than two orders increase already with  $I \sim 100$  pA which must be linked to a transition effect.

Therefore, thermal melting must be examined in the limit of  $I \rightarrow 0$ . Figure 2(e) shows  $r_d(T)|_{I \rightarrow 0}$  in comparison to the  $r_d(T)$  obtained at 20, 40, and 60 pA.  $r_d(T)|_{I \rightarrow 0}$  is well

described as a piecewise behavior across a critical temperature of  $\sim 35$  mK defined as  $T_m$ .  $r_d$  decreases with increasing  $T$  at a rate of 1.5 M $\Omega$ /mK for  $T \leq T_m$ . For  $T \geq T_m$ ,  $r_d$  exhibits an exponential dive marked by nearly four orders of magnitude down to 150 mK. The abrupt change within a few millikelvins of  $T_m$  is referred to as a discontinuity that supports, also confirmed by the zero-field results shown later, a possible first-order phase transition. The piecewise  $r_d(T)$ , however, disappears with  $I$  increased just beyond  $I_c$ . As shown in the inset of Fig. 2(e),  $r_d(T)$  measured between

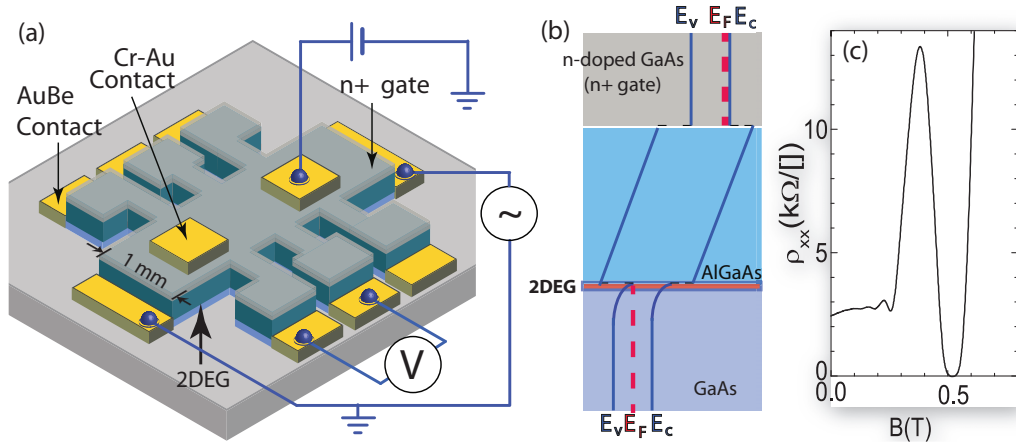


FIG. 3. (a) HIGFET sample and measurement schematics. (b) Band diagram showing accumulation of holes at the GaAs/AlGaAs junction. (c)  $\rho_{xx}(B)$  for  $p = 1.2 \times 10^{10} \text{ cm}^{-2}$ .

20 and 60 pA is substantially suppressed at  $T \leq T_m$  and only smooth nonmonotonic crossovers are found. These results are consistent with what is indicated by the threshold behavior that a phase transition has occurred when  $I > I_c$ .

Meanwhile, although pinning at  $T < T_m$  is consistently strong,  $V_c$  exhibits a noticeable  $T$  dependence. Figure 2(d) shows selected  $IV$ s for 10, 25, 50, 75, and 150 mK within a narrower window. Note that  $r_d$  is now shown as resistivity (instead of resistance). For 10 and 25 mK, current switches on at different thresholds: 0.4 mV for 25 mK and 0.8 mV for 10 mK. Lower  $E_c$  for higher  $T$  is qualitatively consistent with the Lindemann criterion for crystal melting [14]. An estimate of  $\xi$  is provided here, similar to previous studies [18,33], based on a pinning model [34,35] that balances the pinning energy with the electrical potential energy  $U = Nw_c$ .  $w_c = eE_c a \sim 0.024 \mu\text{eV} \ll T$  is the single-particle potential energy.  $N = p\xi^2$  is the number of carriers on a scale of  $\xi$ . For  $T = 25$  mK,  $E_c = V_c/L \sim 8 \text{ mV/cm}$  where  $L = 0.5 \text{ mm}$ . Setting the electrical force  $NeE_c$  equal to the pinning force  $\kappa a$

[17,18],  $\kappa$  being the shear modulus  $0.245e^2 p^{3/2}/4\pi\epsilon_0\epsilon$  [36],  $N \sim 1.5 \times 10^5$  or  $\xi \geq 10 \mu\text{m}$  is obtained.  $U$  is  $\sim 2.4 \text{ meV}$  (or 30 K), comparable to  $E_{ee}$ .

For  $T$  between 40 and 140 mK, the threshold is replaced with a rounded nonlinear  $IV$ . This observation is in agreement with several previous results [17,25–27] which were interpreted as pinned WCs. However,  $E_c$  disappears because a current switches on in the limit of  $V \rightarrow 0$ . In addition, pinning is substantially reduced, i.e.,  $r_d \sim 10 \text{ M}\Omega$  at 50 mK. Therefore, this region should be of an intermediate phase since it crosses over to a liquid above 140 mK (referred to as  $T_l$ ).  $r_d$  for  $T \geq T_l$  is 30–40 k $\Omega/\square$ . The same values of  $r_d$  are found for the liquid phase arrived at by  $E$ -field-driven melting at sufficiently large bias. A suggested phase diagram is shown in Fig. 2(f).

To identify the nature of the intermediate phase is difficult because the exact relationship between  $r_d$  and  $\xi(T)$  has to first be formulated. Here, as a minor point, we show that  $r_d(T)$  can be fitted to  $r_d = r_0 \exp[c/(T - 40 \text{ mK})^\gamma]$  with  $r_0 \approx 23$

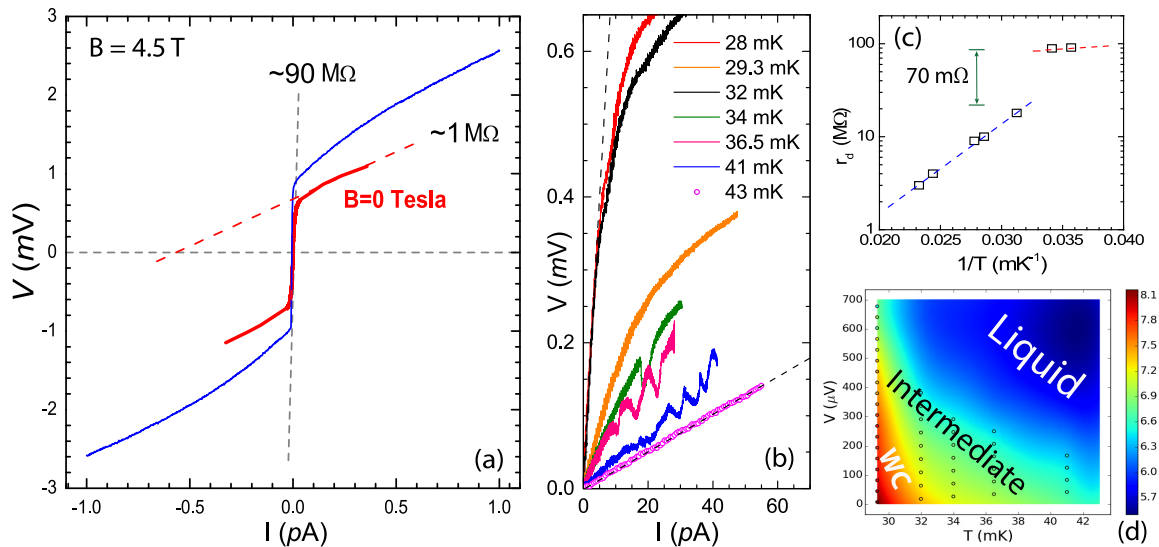


FIG. 4. (a) dc  $IV$  at  $T = 28$  mK. (b)  $IV$ s obtained at different  $T$ . (c)  $T$  dependence of  $r_d(T)|_{V \rightarrow 0}$  on semilogarithmic scales. (d) Colored contour phase diagram based on  $\log_{10} r_d(T)$  values. Dashed lines are guides.

and  $c \approx 9.5$ , in the same trend as the exponentially decreasing  $\xi(T)$  modeled for a hexatic phase [13]:  $\xi \sim \exp[c/(T - T_m)^\gamma]$  ( $\gamma \approx 0.3696$ ).

We now turn to the zero- $B$ -field study with undoped GaAs/AlGaAs HIGFETs [37–39]. A 6 mm  $\times$  0.8 mm Hall bar is realized with a self-align fabrication process [39] [Fig. 3(a)]. Accumulation of holes at the heterointerface is capacitively induced through biasing a top gate beyond a turn-on voltage,  $\sim -1.3$  V, at which the valance band edge meets the chemical potential [Fig. 3(b)]. The band gap of the 600-nm-thick  $\text{Al}_{0.3}\text{Ga}_{0.7}\text{As}$  barrier is  $\sim 2$  eV. Owing to the superior crystal quality, gate leakage remains less than 0.05 pA at all operating bias. Density  $p$ , determined via quantum Hall oscillations [Fig. 3(c)], is tunable from  $4 \times 10^{10}$  down to  $7 \times 10^8$  cm $^{-2}$ .

Accessing  $r_s \geq 40$  requires  $p \leq 4 \times 10^9$  cm $^{-2}$ .  $m^* = 0.25m_0$  is a lower-bound estimate. (Determination of  $m^*$  is difficult because of a complicated dispersion relation associated with the light-heavy hole band mixing and the spin-orbit coupling [40].) It is thus important to exclude disorder-driven localization which easily occurs as phonon-activated hopping  $\rho(T) \sim \rho_0 \exp(T^*/T)^{1/\beta}$  ( $\beta = 1-3$ ) [41,42]. Recent studies of ultraclean systems revealed nonactivated power-law behaviors [38,43,44] of interaction-driven nature that distinguishes from a disorder-driven effect. And, the metal-to-insulator transition (MIT) [45] occurs at lowest carrier densities corresponding to  $r_s \sim 35-40$ . We refer the readers to Refs. [38,43,44,46] for details.

The measured MIT in zero  $B$  (not shown) has a critical density  $p_c = 4 \times 10^9$  cm $^{-2}$ . The following dc results are for  $p = 2.8 \times 10^9$  cm $^{-2}$  (or  $r_s \sim 45$ ) measured between 28 and 45 mK. A current bias, with Keithley 6430 fA source, is employed with a voltage sensing at sub- $\mu$ V resolution at an input impedance of  $10^{16}$   $\Omega$ . Figure 4(a) shows a similar threshold  $IV$  obtained at 28 mK, qualitatively identical to the RIP case.  $I_c$  is  $\sim 4$  pA. Strong subthreshold pinning is marked by a  $r_d$  of 90 M $\Omega/\square$ . The suprathreshold  $r_d$  collapses 100 times.  $I_c$  corresponds to a  $E_c \sim 4$  mV/cm (or  $\sim 10^{-10}$  V/ $a_B$ ), yielding a slightly larger single-particle potential energy of  $\sim eE_c a \sim 0.04$   $\mu$ eV (or 0.46 mK) due to the larger  $a \sim 100$  nm. Setting  $NeE_c = \kappa a$  as shown earlier, one obtains  $N \sim 1 \times 10^5$ , corresponding to a substantial scale of  $\xi \sim 100$   $\mu$ m. This yields a dominating potential energy  $U \sim 20$  meV  $> E_{ee}$  which is consistent with a crystal. For a consistency check, the same setup is used to

measure the RIP and the result is shown as the blue curve. The power dissipation is  $\leq 2 \times 10^{-16}$  W, ruling out appreciable Joule heating.

Melting probed by  $r_d|_{I \rightarrow 0}$  is shown in Fig. 4(c) where a piecewise behavior appears across  $T_m \sim 30$  mK.  $dr_d/dT$  is 4 M $\Omega$ /mK for  $T < T_m$ .  $r_d$  exhibits a sharp jump of 70 M $\Omega$  at  $T_m$  above which an exponential  $T$  dependence is found.  $E_c$  disappears at  $T > T_m$  where rounded nonlinear  $IV$  is found. The discontinuous jump resembles a recent quantum Monte Carlo simulation for a first-order WC-intermediate phase transition mediated by a discontinuous internal energy jump [10], and supports a singularity dividing a WC from an intermediate phase. Linear  $IV$  is recovered at  $T_l \sim 42$  mK, noticeably lower than the RIP case. Smaller  $T_m$  and  $T_l$  for the ultradilute case is qualitatively consistent with stronger quantum fluctuations and disorder fluctuations (due to lack of screening). A phase diagram is suggested in Fig. 4(d).

Increasing  $E$ -field results in a switch-on of current and a settlement of  $r_d$  belonging to a liquid phase. Identical to the RIP case, a melting mediated by an intermediate phase is supported. However, there is a noticeable difference in the intermediate phase at  $T > T_m$ :  $V$  oscillates with increasing  $I$  at approximately 5–10 pA spacing. It occurs more frequently as  $T$  approaches  $T_l$  [Fig. 4(b)]. The formation of stripes with long-range orientational order [13], as seen in electrons on a helium surface [47], could be a possible cause. Another possibility is that small  $T_l$  facilitates a melting and recrystallization of pinned WC domains, instead of or in addition to shearing, when driven across pinning sites [48]. This will contribute to a negative  $r_d$ .

To summarize, enormous pinning modes below  $T_m$  support a WC on large  $\xi$  scales. A melting is captured as a two-stage SLT. The WC-intermediate phase transition is likely first-ordered [10] because of the discontinuity in  $r_d$  as well as the disappearance of  $E_c$  above  $T_m$ . Results obtained from both RIP and zero- $B$ -field studies are remarkably consistent. The small  $T_m$ , which is  $\sim (1/7)T_{cm}$ , suggests strong effects from system disorders and quantum fluctuations that require further understanding.

This work is supported by NSF under Grant No. DMR-1410302, and by the Gordon and Betty Moore Foundation through Grant No. GBMF2719, and NSF Grant No. MRSEC-DMR-0819860.

- 
- [1] E. Wigner, *Phys. Rev.* **46**, 1002 (1934).  
 [2] N. D. Mermin and H. Wagner, *Phys. Rev. Lett.* **17**, 1133 (1966).  
 [3] N. D. Mermin, *Phys. Rev.* **176**, 250 (1968).  
 [4] J. Kosterlitz and D. Thouless, *J. Phys. C* **5**, L124 (1972).  
 [5] B. Tanatar and D. M. Ceperley, *Phys. Rev. B* **39**, 5005 (1989).  
 [6] P. W. Anderson, *Phys. Rev.* **109**, 1492 (1958).  
 [7] H. Aoki, *J. Phys. C* **12**, 633 (1979).  
 [8] P. Anderson, *Basic Notions of Condensed Matter Physics* (Benjamin/Cummings, Menlo Park, CA, 1984).  
 [9] M. Takahashi and M. Imada, *J. Phys. Soc. Jpn.* **53**, 3765 (1984).  
 [10] B. K. Clark, M. Casula, and D. M. Ceperley, *Phys. Rev. Lett.* **103**, 055701 (2009).  
 [11] J. M. Kosterlitz and D. J. Thouless, *J. Phys. C* **6**, 1181 (1973).  
 [12] B. I. Halperin and D. R. Nelson, *Phys. Rev. Lett.* **41**, 121 (1978).  
 [13] D. R. Nelson and B. I. Halperin, *Phys. Rev. B* **19**, 2457 (1979).  
 [14] G. M. Bruun and D. R. Nelson, *Phys. Rev. B* **89**, 094112 (2014).  
 [15] A. P. Young, *Phys. Rev. B* **19**, 1855 (1979).  
 [16] H. W. Jiang, H. L. Stormer, D. C. Tsui, L. N. Pfeiffer, and K. W. West, *Phys. Rev. B* **44**, 8107 (1991).  
 [17] V. J. Goldman, M. Santos, M. Shayegan, and J. E. Cunningham, *Phys. Rev. Lett.* **65**, 2189 (1990).  
 [18] F. I. B. Williams, P. A. Wright, R. G. Clark, E. Y. Andrei, G. Deville, D. C. Glatli, O. Probst, B. Etienne, C. Dorin, C. T. Foxon, and J. J. Harris, *Phys. Rev. Lett.* **66**, 3285 (1991).

- [19] E. Y. Andrei, G. Deville, D. C. Glattli, F. I. B. Williams, E. Paris, and B. Etienne, *Phys. Rev. Lett.* **60**, 2765 (1988).
- [20] Y. P. Chen, G. Sambandamurthy, Z. H. Wang, R. M. Lewis, L. W. Engel, D. C. Tsui, P. D. Ye, L. N. Pfeiffer, and K. W. West, *Nat. Phys.* **2**, 452 (2006).
- [21] H. Zhu, Y. P. Chen, P. Jiang, L. W. Engel, D. C. Tsui, L. N. Pfeiffer, and K. W. West, *Phys. Rev. Lett.* **105**, 126803 (2010).
- [22] M. A. Paalanen, R. L. Willett, P. B. Littlewood, R. R. Ruel, K. W. West, L. N. Pfeiffer, and D. J. Bishop, *Phys. Rev. B* **45**, 11342 (1992).
- [23] J. Jang, B. M. Hunt, L. N. Pfeiffer, K. W. West, and R. C. Ashoori, *Nat. Phys.* **13** 340 (2017).
- [24] D. R. Nelson and B. I. Halperin, *Phys. Rev. B* **21**, 5312 (1980).
- [25] S. V. Kravchenko, J. A. A. J. Perenboom, and V. M. Pudalov, *Phys. Rev. B* **44**, 13513 (1991).
- [26] V. M. Pudalov, M. D'Iorio, S. V. Kravchenko, and J. W. Campbell, *Phys. Rev. Lett.* **70**, 1866 (1993).
- [27] J. Yoon, C. C. Li, D. Shahar, D. C. Tsui, and M. Shayegan, *Phys. Rev. Lett.* **82**, 1744 (1999).
- [28] M. Y. Simmons, A. R. Hamilton, M. Pepper, E. H. Linfield, P. D. Rose, D. A. Ritchie, A. K. Savchenko, and T. G. Griffiths, *Phys. Rev. Lett.* **80**, 1292 (1998).
- [29] J. Huang, J. S. Xia, D. C. Tsui, L. N. Pfeiffer, and K. W. West, *Phys. Rev. Lett.* **98**, 226801 (2007).
- [30] T. Sajoto, Y. P. Li, L. W. Engel, D. C. Tsui, and M. Shayegan, *Phys. Rev. Lett.* **70**, 2321 (1993).
- [31] M. Hilke, D. Shahar, S. Song, D. Tsui, Y. Xie, and D. Monroe, *Nature (London)* **395**, 675 (1998).
- [32] G. Grüner, *Rev. Mod. Phys.* **60**, 1129 (1988).
- [33] V. J. Goldman, M. Shayegan, and D. C. Tsui, *Phys. Rev. Lett.* **61**, 881 (1988).
- [34] P. A. Lee and H. Fukuyama, *Phys. Rev. B* **17**, 542 (1978).
- [35] H. Fukuyama and P. A. Lee, *Phys. Rev. B* **17**, 535 (1978).
- [36] L. Bonsall and A. Maradudin, *Phys. Rev. B* **15**, 1959 (1977).
- [37] B. E. Kane, L. N. Pfeiffer, and K. W. West, *Appl. Phys. Lett.* **67**, 1262 (1995).
- [38] H. Noh, M. P. Lilly, D. C. Tsui, J. A. Simmons, E. H. Hwang, S. Das Sarma, L. N. Pfeiffer, and K. W. West, *Phys. Rev. B* **68**, 165308 (2003).
- [39] J. Huang, D. S. Novikov, D. C. Tsui, L. N. Pfeiffer, and K. W. West, *Int. J. Mod. Phys. B* **21**, 1219 (2007).
- [40] R. Winkler, *Spin–Orbit Coupling Effects in Two-Dimensional Electron and Hole Systems* (Springer, New York, 2003).
- [41] N. F. Mott, *Philos. Mag.* **19**, 835 (1969).
- [42] A. L. Efros and B. I. Shklovskii, *J. Phys. C* **8**, L49 (1975).
- [43] J. Huang, D. S. Novikov, D. C. Tsui, L. N. Pfeiffer, and K. W. West, *Phys. Rev. B* **74**, 201302 (2006).
- [44] J. Huang, L. N. Pfeiffer, and K. W. West, *Phys. Rev. B* **85**, 041304 (2012).
- [45] S. V. Kravchenko, W. E. Mason, G. E. Bowker, J. E. Furneaux, V. M. Pudalov, and M. D'Iorio, *Phys. Rev. B* **51**, 7038 (1995).
- [46] J. Huang, L. N. Pfeiffer, and K. W. West, *Phys. Rev. Lett.* **112**, 036803 (2014).
- [47] P. Glasson, V. Dotsenko, P. Fozooni, M. J. Lea, W. Bailey, G. Papageorgiou, S. E. Andresen, and A. Kristensen, *Phys. Rev. Lett.* **87**, 176802 (2001).
- [48] B. G. A. Normand, P. B. Littlewood, and A. J. Millis, *Phys. Rev. B* **46**, 3920 (1992).